

Topology of pulsating active matter: Defect asymmetry controls emergent motility

Luca Casagrande,^{1,*} Alessandro Manacorda,^{1,2} and Étienne Fodor^{1,†}

¹*Department of Physics and Materials Science, University of Luxembourg, L-1511 Luxembourg City, Luxembourg*

²*CNR Institute of Complex Systems, Uos Sapienza, Piazzale A. Moro 5, 00185 Rome, Italy*

In pulsating active matter, topological defects are motile despite the absence of any macroscopic flows and microscopic self-propulsion. We reveal that this motility arises from a ratchet effect: the mechanochemical coupling between local oscillations and repulsive interactions breaks both spatial and time-reversal symmetries, thus leading asymmetric rotating defects to drift under fluctuations. This mechanism regulates a crossover between spiral waves connecting slow defects and fiber-like waves connecting fast defects, in analogy with the onset of heart rhythm disorder in cardiac tissues. We rationalize this crossover in terms of a fluctuating hydrodynamics that captures how motile defects spontaneously nucleate and move within an ordered background.

Introduction.—Pulsating active particles subject to periodic mechanical deformations have garnered increasing attention [1–13]. They capture collective effects in deformation-driven soft media [14], some of which play an important role in living systems [15–22]. For instance, excitation waves in cardiac tissues organize dynamical patterns around topological defects [23–25]. During cardiac arrhythmia, the crossover from tachycardia to fibrillation changes these patterns from stable spirals with steady defects to fiber-like waves with motile defects [26]. Similarly, deformation waves in pulsating active matter yield motile defects connected by spiral and fiber-like waves [Figs. 1-2]. The principles underlying these defect dynamics have remained largely elusive.

Defects help rationalize the mechanisms of pattern formation [27–30]. In cardiac and excitable systems, defect dynamics has been characterized theoretically and experimentally [31–38]. In nematic and polar active matter, asymmetric defects can spontaneously move and generate flows that sustain large-scale vortices [39–47]. Similarly, motile dislocations are present in active smectics [48] and odd crystals [49], while motile defects have been reported in driven XY [50] and nonreciprocal systems [51]. In pulsating active matter, it remains to elucidate how defects move despite the absence of any macroscopic flows and microscopic self-propulsion.

In this Letter, we reveal that defect motility emerges from a ratchet effect [53–56]. The mechanochemical coupling between size oscillations and repulsion leads to asymmetric defect cores that drift under fluctuations. Our hydrodynamics captures the relevant broken spatial and time-reversal symmetries to rationalize how defect asymmetry controls motility. Overall, our symmetry arguments elucidate how repulsion and pulsation regulate the crossover between spiral and fiber-like waves, with direct implications for cardiac arrhythmia [23–25].

Topology of pulsating active matter.—We consider N pulsating particles in a periodic box of size L with positions \mathbf{r}_i and phases ϕ_i . The phases effectively represent chemical cycles internal to each particle [3, 11, 19]. Particle sizes $\sigma_i = \sigma_0(1 + \lambda \sin \phi_i)/(1 + \lambda)$ are determined by their phases ϕ_i , where $\sigma_0 = 1$ is a reference size, and

$\lambda < 1$ sets the amplitude of deformation. Positions and phases follow overdamped Langevin dynamics [6]:

$$\begin{aligned} \dot{\mathbf{r}}_i &= -\mu_r \nabla_i U + \sqrt{2D_r} \boldsymbol{\xi}_i, \\ \dot{\phi}_i &= \omega - \mu_\phi \partial_{\phi_i} U + \sum_j \varepsilon_{ij} \sin(\phi_j - \phi_i) + \sqrt{2D_\phi} \eta_i. \end{aligned} \quad (1)$$

The synchronization strength is $\varepsilon_{ij} = \varepsilon$ for $a_{ij} < 1$, where $a_{ij} = |\mathbf{r}_i - \mathbf{r}_j|/(\sigma_i + \sigma_j)$, and $\varepsilon_{ij} = 0$ otherwise. The drive ω favors periodic pulsation of sizes, while (μ_r, μ_ϕ) and (D_r, D_ϕ) are the mobility and diffusion coefficients, respectively. The Gaussian white noise terms $(\boldsymbol{\xi}_i, \eta_i)$ are uncorrelated with zero mean.

The repulsive potential $U = \frac{1}{2} \sum_{i,j} U_0(a_{ij}^{-12} - 2a_{ij}^{-6} + 1)$ has a cut-off at $a_{ij} = 1$. The dependence of U on positions \mathbf{r}_i and phases ϕ_i yields displacement $(-\nabla_i U)$ and deformation $(-\partial_{\phi_i} U)$ forces when particles overlap. This mechanochemical coupling is typically absent when modelling contractile tissues as excitable media [31, 34–37], and implies that U is not invariant under an arbitrary

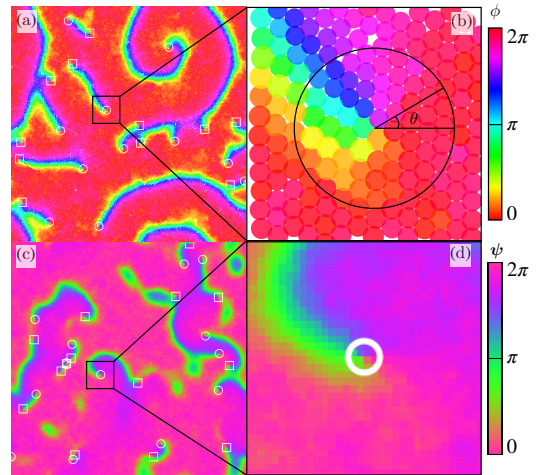


FIG. 1. Deformation waves connect defects that rotate with asymmetric cores for (a,b) pulsating particles [Eq. (1)], and (c,d) fluctuating hydrodynamics [Eq. (8)]. The rotation is set by defect charges +1 (o, CW) and -1 (□, CCW), while profile asymmetry is similar for ± 1 defects. Parameters in Ref. [52].

rotation of phases ϕ_i . In what follows, we reveal that the broken invariance induced by mechanochemical coupling plays a crucial role in regulating defect motility.

The phase diagram features three homogeneous states: disorder (no synchronization), cycles (synchronization with phase current), and arrest (synchronization without phase current) [6]. In between the regimes of cycles and arrest, a dynamical instability leads to deformation waves that propagate coordinated changes in phases ϕ_i with negligible displacement of positions \mathbf{r}_i . Topological defects of opposite charges $\frac{1}{2\pi} \oint d\phi = \pm 1$ rotate clockwise/counterclockwise (depending on their charges), and are connected by pairs through waves [Figs. 1(a-b)]; the connectivity of these pairs changes whenever waves collide. In what follows, we examine in detail how waves self-organize into various patterns associated with distinct defect statistics.

Increasing the density $\rho = N/L^2$, we observe that *spirals*, where defects are connected through long waves, turn into *fibers* with a shorter distance between connected defects [Figs. 2(a-d)]. Similar spirals can be found in other models, such as reaction-diffusion dynamics described by the complex Ginzburg-landau equation (CGLE [57]). At small ρ , neglecting the repulsive term $\partial_{\phi_i} U$ in the phase dynamics [Eq. (1)] yields a noisy Kuramoto model [58] (analogously, a driven XY model [59]) that maps into CGLE. In contrast, the fibers do not admit any straightforward analogy with patterns of CGLE. Indeed, the term $\partial_{\phi_i} U$ breaks the rotational invariance of the phase dynamics, so that the phases arrest and waves cannot propagate if ρ exceeds a threshold ρ_c [52]. At intermediate ρ , the emergence of waves stems from local excitations nucleating on an arrested background.

Defect displacement drastically changes between spirals and fibers. The mean-squared average $\langle \Delta x^2 \rangle$ of displacement $\Delta x(t) = |\mathbf{x}(t+t_o) - \mathbf{x}(t_o)|$ shows that defects move slower (i.e., smaller $\langle \Delta x^2 \rangle$ at large t) and rotate faster (i.e., oscillating $\langle \Delta x^2 \rangle$ at small t) for large $1 - \rho/\rho_c$ [Fig. 2(e)]. In other words, spirals are associated with slow-moving, fast-rotating defects, whereas fibers come with fast-moving, slow-rotating defects.

The distribution $P(v)$ of defect velocity $v(t) = \Delta x(t)/t$, normalized as $\int_0^\infty v P(v) dv = 1$ with isotropic symmetry, exhibits peaks that signal defect motility [Fig. 2(f)]; we measure $v(t)$ for a time interval t smaller than the typical time for defects to complete a rotation (that corresponds to the first oscillation in $\langle \Delta x^2 \rangle$). At high ρ , defects hop along a lattice formed by the particle close packing, so $P(v)$ features several peaks corresponding to discrete jumps [52]. For comparison, the velocity statistics of inertial Brownian particles (without motility, with mass m and temperature T) follows the Boltzmann weight $P(v) \sim e^{-mv^2/(2T)}$ centered at $v = 0$. Here, motile defects stabilize despite the absence of any self-propulsion in the microscopic dynamics [Eq. (1)]: instead, defect motility stems from an emergent mechanism

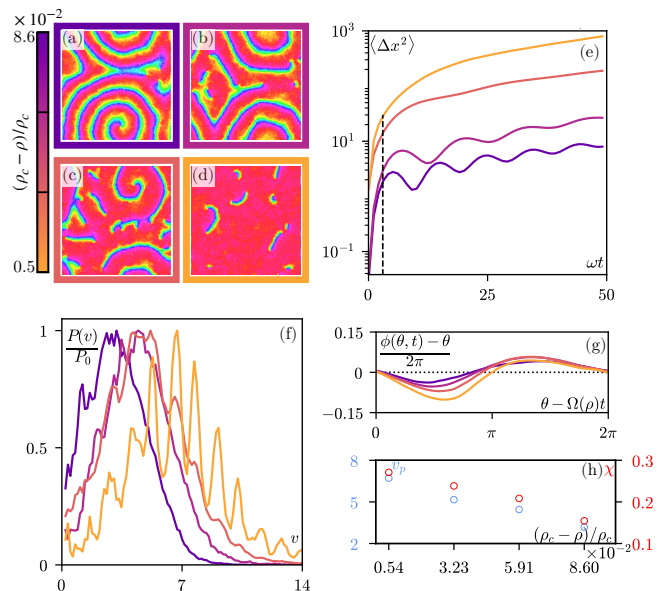


FIG. 2. Defect statistics for pulsating particles [Eq. (1)]. (a)–(d) Phase patterns change from spirals to fiber-like waves as density ρ increases; color code and parameters as in Fig. 1(a). (e) Mean-squared displacement $\langle \Delta x^2 \rangle$ of defect cores as a function of time t ; colors refer to ρ values, and dashed line to time interval at which velocity is estimated. (f) Defect velocity distribution $P(v)$ of scaled by $P_0 = \max P(v)$. (g) Defect profile $\phi(\theta, t)$ in the co-rotating frame $\theta - \Omega(\rho)t$. (h) Peak velocity $v_p = \text{argmax} P(v)$ and asymmetry factor $\chi[\phi]$ [Eq. (2)].

associated with pattern formation.

Defect displacement has been related to shape asymmetry in various types of active matter [28]. Here, we characterize such an asymmetry by considering the rotating phase profile $\phi(\theta, t)$ as a function of the polar angle θ [Fig. 1(b)] [52]. In the frame rotating at frequency Ω , the asymmetry of the profile $\phi(\theta - \Omega t)$ increases with ρ [Fig. 2(g)]: defect cores are more symmetric for spirals than for fibers. In fact, the asymmetry factor

$$\chi[\phi] = \frac{1}{2\pi} \int_0^{2\pi} |\phi(\theta) - \theta| d\theta \quad (2)$$

correlates with the peak value of velocity distribution $v_p = \text{argmax} P(v)$ [Fig. 2(h)], showing that χ is a reliable predictor of defect motility.

In short, the topology of deformation waves obeys a crossover between spirals and fibers with distinct defects. Defect charge sets wave rotation, and the asymmetry factor χ suffices to distinguish between fast-moving, slow-rotating and slow-moving, fast-rotating defects. In what follows, we develop a hydrodynamic theory that helps rationalize how to control motility through asymmetry.

Broken invariance in fluctuating hydrodynamics.—We coarse-grain our microscopic dynamics to study pattern and defect formation through a large-wavelength description. Specifically, our aim is to obtain a closed dynamics

for the complex field $A(\mathbf{r}, t)$ that quantifies the local degree of phase synchronization:

$$A(\mathbf{r}, t) = \frac{1}{\rho} \sum_j e^{i\phi_j(t)} \delta(\mathbf{r} - \mathbf{r}_j(t)) = R e^{i\psi}. \quad (3)$$

For simplicity, we discard interactions in the position dynamics, so that ρ remains constant. We also approximate repulsion in the phase dynamics as an external field that favors small size: $\partial_{\phi_i} U \approx h(\rho) \cos \phi_i$, where $h(\rho) = \rho^6$. We demonstrate below that these approximations enable a systematic hydrodynamic derivation that retains the essential features at play in defect motility.

Stochastic calculus [60, 61] yields the dynamics of the angular moments $f_n(\mathbf{r}, t) = \int e^{in\phi} P(\phi, \mathbf{r}, t) d\phi$ derived from the empirical distribution $P(\phi, \mathbf{r}, t) = \sum_j \delta(\phi - \phi_j(t)) \delta(\mathbf{r} - \mathbf{r}_j(t))$:

$$\begin{aligned} \partial_t f_n &= (D_r \nabla^2 + in\omega - n^2 D_\phi) f_n - inh(\rho)(f_{n+1} + f_{n-1}) \\ &\quad + (n\varepsilon/2)(f_1 f_{n-1} - f_{-1} f_{n+1}) + \sqrt{2D_\phi} \Lambda_n. \end{aligned} \quad (4)$$

The noise $\Lambda_n = u_n + iv_n$ is Gaussian with correlations

$$\begin{aligned} \langle (u_n, v_n)(\mathbf{r}, t) (u_n, v_n)^T(\mathbf{r}', t') \rangle &= \mathbb{C}_n \delta(\mathbf{r} - \mathbf{r}') \delta(t - t'), \\ \mathbb{C}_n &= \frac{1}{2} \begin{pmatrix} f_0 - \text{Re}[f_{2n}] & -\text{Im}[f_{2n}] \\ -\text{Im}[f_{2n}] & f_0 + \text{Re}[f_{2n}] \end{pmatrix}. \end{aligned} \quad (5)$$

In practice, we generate (u_n, v_n) with two Gaussian white noises using a Cholesky decomposition of \mathbb{C}_n [52]. The hierarchy in Eq. (4) needs to be combined with a specific closure to deduce the dynamics of $A = f_1/\rho$.

Some closures in coarse-graining active models involve an adiabatic elimination of higher-order moments that is valid only close to disorder [62, 63]. When deploying this strategy to pulsating active matter, it proved inadequate to properly capture the emergence of motile defects [6]. Instead, inspired by [64–67], we use the closure $P(\phi, \mathbf{r}, t) \approx P_{\text{ans}}(\phi | \psi(\mathbf{r}, t), \kappa(\mathbf{r}, t))$ with the ansatz

$$P_{\text{ans}}(\phi | \psi, \kappa) = (\rho/\kappa) H(\kappa/2 - |\psi - \phi|), \quad (6)$$

where $H(x > 0) = 1$ and $H(x < 0) = 0$, leading to

$$f_n(\mathbf{r}, t) = \rho e^{in\psi(\mathbf{r}, t)} \text{sinc} \left(\frac{n\kappa(\mathbf{r}, t)}{2} \right). \quad (7)$$

The ansatz P_{ans} parametrizes the distribution in terms of mean ψ and variance κ to distinguish the three homogeneous states: disorder ($\kappa = 2\pi$), cycles ($\kappa < 2\pi$ and $\psi \neq 0$), and arrest ($\kappa < 2\pi$ and $\psi = 0$) [Fig. 3(a)]. In general, (ψ, κ) are space-dependent fields whose realizations determine all the angular moments $f_n = f_n(\psi, \kappa)$ [Eq. (7)]. Our closure enforces that f_n is determined by f_1 (a similar strategy is used for space-independent oscillators [68–72]) under the constraint $|f_n| < \rho$ ensuring stability of noise correlations: $\det \mathbb{C}_n > 0$ [Eq. (5)].

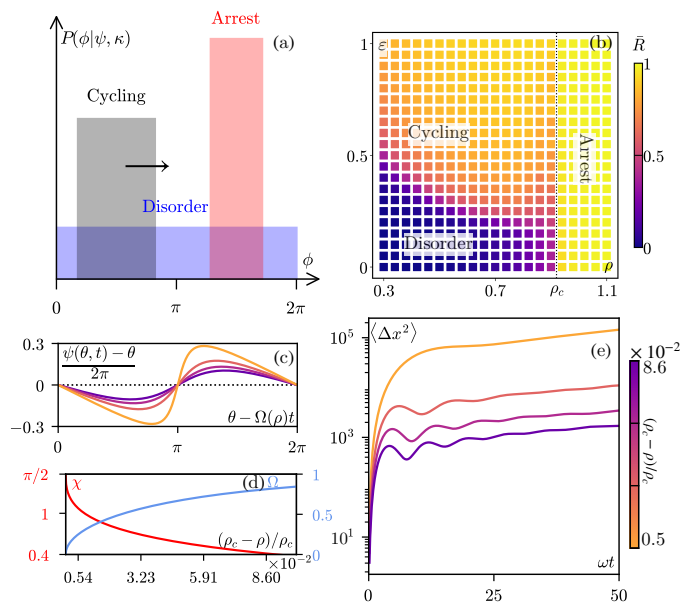


FIG. 3. Fluctuating hydrodynamics [Eq. (8)]. (a) Schematic of the ansatz distribution $P_{\text{ans}}(\phi | \psi, \sigma)$ [Eq. (6)]. (b) Phase diagram: $\bar{R} = \frac{1}{V} \int_V R(\mathbf{r}) d\mathbf{r}$ [Eq. (3)] as a function of density ρ and synchronization ε . (c) Analytical defect profile $\psi(\theta, t)$ [Eq. (11)] in the co-rotating frame $\theta - \Omega(\rho)t$; colors refer to ρ values. (d) Corresponding asymmetry factor $\chi[\psi]$ [Eq. (2)] and rotational frequency Ω [Eq. (12)]. (e) Mean-squared displacement $\langle \Delta x^2 \rangle$ in effective defect dynamics [Eq. (13)]. Parameters in Ref. [52].

The expressions $f_1 = f_1(\psi, \kappa)$ and $f_2 = f_2(\psi, \kappa)$ define a closed relation between the first and second moments: $f_2 = f_2(f_1)$. The dynamics for A then directly follows from Eq. (4) in the case $n = 1$:

$$\partial_t A = D_r \nabla^2 A + F(A) + G(A) + \sqrt{2D_\phi} (\Lambda_1/\rho), \quad (8)$$

where

$$\begin{aligned} F(A) &= (i\omega + \varepsilon\rho/2 - D_\phi)A - (\varepsilon\rho/2)A^* f_2(A), \\ G(A) &= ih(\rho)[1 + f_2(A)/\rho], \end{aligned} \quad (9)$$

and A^* is the complex conjugate of A . Under arbitrary rotation Φ of the complex phase, $F(A)$ is symmetric as in CGLE [57], while $G(A)$ is not: $F(Ae^{i\Phi}) = e^{i\Phi} F(A)$, and $G(Ae^{i\Phi}) \neq e^{i\Phi} G(A)$, where we have used $f_2(Ae^{i\Phi}) = e^{i2\Phi} f_2(A)$. Since $G(A)$ is proportional to the field $h(\rho)$ that embodies microscopic repulsion, this term describes how repulsion regulates the deviation of our hydrodynamics from that of rotation-invariant synchronization theories. Terms breaking rotational invariance have also been reported in the hydrodynamics of Ref. [6], albeit with a series of caveats. We discuss below how our hydrodynamics solve these issues, and open the door to studying defect motility.

Our hydrodynamic phase diagram [Fig. 3(b)] features the three homogeneous states (disorder, cycles, arrest) as

in microscopies [6]. These phases bare analogies with recent theories [73–75] at mean-field level, namely without space and noise. In the ordered state [$A \approx e^{i\psi}$, Eq. (3)], arrest emerges above the critical density ρ_c defined by $h(\rho_c) = \omega$ [52]. We do not observe the spurious counter-clockwise cycling reported in Ref. [6], which was recognized as an artifact of the adiabatic elimination. Between arrest and cycles, a regime of instability leads motile defects to nucleate and propagate in the arrested background [Figs. 1(c-d)]. As in microscopies [Figs. 1(a-b)], defect profiles are strongly asymmetric, and defect pairs are connected by fibers; Ref. [6] missed such asymmetric defects at the hydrodynamic level.

Fluctuations play an essential role in stabilizing hydrodynamic patterns. Homogeneous states are linearly stable [52], yet the presence of the noise term Λ_1 [Eq. (8)] destabilizes homogeneous profiles and selects defect profiles in our numerics. The success of our hydrodynamics stems from carefully deriving (and simulating) the multiplicative noise [Eq. (5)] consistently with our closure [Eq. (7)]. In contrast, the additive noise in the hydrodynamics of Ref. [6] is inadequate to capture the nucleation of asymmetric defects in an arrested background.

In short, our fluctuating hydrodynamics captures emergent motile defects with asymmetric profiles, thus going beyond the hydrodynamic description in Ref. [6]. We now exploit this revised hydrodynamics to examine the mechanism at play in defect motility.

Ratchet effect controls emergent defect motility.—The emergence of motile defects is an instance of the ratchet effect [53–56]: it stems from simultaneously breaking the spatial symmetry of defect profiles, as seen in other active defects [28], and the time-reversal symmetry of the dynamics [76–78], here due to pulsation. In what follows, we leverage our hydrodynamics to explicitly relate defect asymmetry and emergent motility.

We proceed with a series of approximations to derive the profile of the phase ψ [Eq. (3)] around defects. Defects evolve in an ordered background, so we consider the solution $A \approx e^{i\psi}$ in our hydrodynamics [Eq. (8)]:

$$\partial_t \psi = \frac{D_r}{r^2} \partial_{\theta\theta} \psi + \omega - h(\rho) \cos \psi, \quad (10)$$

where (r, θ) are the polar coordinates in the co-moving frame [Fig. 1], and we have assumed that ψ depends only on θ close to defect cores. Rotating solutions exist at small density $\rho < \rho_c$, namely for high pulsation $\omega > h(\rho)$. In the frame rotating at frequency $\Omega(\rho)$, we deduce the defect profile in the regime $r \gg \sqrt{D_r/\Omega(\rho)}$ [52]:

$$\psi(\theta, t) = 2 \arctan \left[\tan \left(\frac{\theta - \Omega(\rho)t}{2} \right) \frac{\Omega(\rho)}{\omega + h(\rho)} \right], \quad (11)$$

where the rotational frequency reads

$$\Omega(\rho) = q \sqrt{\omega^2 - h^2(\rho)}, \quad (12)$$

for a defect charge $q = \pm 1$. As ρ gets closer to the arrested value ρ_c , namely ω approaches $h(\rho)$, we observe the same trend as in microscopies [Fig. 2].

First, the profile ψ gets more asymmetric [Fig. 3(c)], as shown by $\chi[\psi]$ [Eq. (2)] [Fig. 3(d)], which in turn increases defect motility by virtue of the ratchet effect [53–56]. Second, the frequency Ω decreases [Fig. 3(d)]; the divergence of the period $T = 2\pi/\Omega$ [Fig. 3(d)] close to arrest, namely for $\omega = h(\rho)$, is common to saddle-node-infinite-period (SNIPER) bifurcations [74, 75]. In short, our hydrodynamics accommodates defects that rotate slower and move faster with density, as in microscopies.

We now offer an effective defect dynamics informed by the profile ψ [Eq. (11)] that captures the displacement statistics reported in microscopies [Fig. 2]. The displacement results from the interplay between emergent motility (driven by asymmetric cores), intrinsic defect rotation, and defect interactions. Therefore, we map our defects into chiral motile particles [79] with position \mathbf{x} and orientation $\hat{\mathbf{e}}(\theta) = (\cos \theta, \sin \theta)$:

$$\dot{\mathbf{x}} = \nu(\rho) \hat{\mathbf{e}}(\theta), \quad \dot{\theta} = \Omega(\rho) + \sqrt{2/\tau} \eta, \quad (13)$$

where ν is the motility, Ω the chirality, and τ the orientation persistence [61]. We map Ω into the rotational frequency of the asymmetric profile [Eq. (12)]. The Gaussian noise η has zero mean and unit correlations. Defect motility emerges at one-body level due to asymmetric cores; in contrast, symmetric defects in CGLE move only through interactions [80, 81]. We expect defect interactions to renormalize $\nu(\rho)$.

In microscopies, the numerical evaluation of peak velocity $v_p(\rho)$ and defect asymmetry $\chi(\rho)$ [Fig. 2(h)] provides the relation $v_p = v_p(\chi)$. We leverage this relation to evaluate $\nu = \nu(\chi)$ in terms of the asymmetry $\chi[\psi]$ of the hydrodynamic defect profile ψ [Eq. (11)]. This procedure yields the explicit dependence $\nu(\rho)$ [52]. The corresponding mean-squared displacement $\langle \Delta x^2 \rangle$ for the effective dynamics [Eq. (13)] captures the same crossover as in microscopies [Fig. 2(e)]: defects change from slow-moving, fast-rotating to fast-moving, slow-rotating dynamics as ρ increases [Fig. 3(e)]. In fact, slow-rotating defects move faster with ρ because of both larger motility $\nu(\rho)$ and smaller chirality $\Omega(\rho)$.

In short, the ratchet effect relates asymmetric profiles with emergent motility of defects. The corresponding defect dynamics features a crossover between two regimes of defect displacement that mirrors the change from spiral to fiber-like waves in microscopies.

Discussion.—In pulsating active matter, the coupling between phases and positions is essential: it yields forces that break rotational invariance, which in turn stabilize patterns and defects distinct from the standard phenomenology of rotation-invariant synchronization theories [57, 58]. Specifically, asymmetric defects regulate the self-organization of deformation waves into steady

spirals and fiber-like patterns that bear analogies with the physics of cardiac tissues [23–25].

We have revealed that the asymmetric profile and the displacement statistics of defects hold the signature of the crossover between spirals and fibers. Using a hydrodynamic description, we have unveiled the broken symmetries that regulate this crossover through a ratchet effect. Our approach uncovers the key role of large-scale fluctuations: it destabilizes order by nucleating defects that behave as motile chiral particles. The closure of our coarse-graining can inspire novel hydrodynamic derivations in other classes of active matter [62, 63, 82].

The ability to predict and control defect dynamics has broad implications. Control theory offers a roadmap to manipulate nonequilibrium patterns [83–88] and guide strategies for steering defects towards desired configurations [89–93]. A derivation of defect interactions, inspired by recent works [45, 94–97], would be a fruitful starting point for a control framework in pulsating active matter.

We acknowledge insightful discussions with Francesco Serafin and Yiwei Zhang. This project has received funding from the European Union’s Horizon Europe research and innovation programme under the Marie Skłodowska-Curie grant agreement No 101056825 (NewGenActive), and from the Luxembourg National Research Fund (FNR), grant references 17962137 and 14389168. A.M. acknowledges financial support from Grant No. 2022HNW5YL MOCA funded by the Ministero dell’Università e della Ricerca PRIN2022 program.

* luca.casagrande@uni.lu

† etienne.fodor@uni.lu

- [1] E. Tjhung and L. Berthier, Discontinuous fluidization transition in time-correlated assemblies of actively deforming particles, *Phys. Rev. E* **96**, 050601(R) (2017).
- [2] Y. Koyano, H. Kitahata, and A. S. Mikhailov, Diffusion in crowded colloids of particles cyclically changing their shapes, *Europhys. Lett.* **128**, 40003 (2020).
- [3] Y. Togashi, Modeling of nanomachine/micromachine crowds: Interplay between the internal state and surroundings, *J. Phys. Chem. B* **123**, 1481 (2019).
- [4] D. R. Parisi, L. E. Wiebke, J. N. Mandl, and J. Textor, Flow rate resonance of actively deforming particles, *Sci. Rep.* **13**, 9455 (2023).
- [5] Z.-Q. Li, Q.-L. Lei, and Y. qiang Ma, Fluidization and anomalous density fluctuations in 2d voronoi celepithelial tissues with pulsating activity, *Proc. Natl. Acad. Sci. USA* **122**, e2421518122 (2025).
- [6] Y. Zhang and E. Fodor, Pulsating active matter, *Phys. Rev. Lett.* **131**, 238302 (2023).
- [7] W. h. Liu, W. j. Zhu, and B. q. Ai, Collective motion of pulsating active particles in confined structures, *New J. Phys.* **26**, 023017 (2024).
- [8] W. D. Piñeros and E. Fodor, Biased ensembles of pulsating active matter, *Phys. Rev. Lett.* **134**, 038301 (2025).
- [9] T. Banerjee, T. Desaleux, J. Ranft, and 'Etienne Fodor, *Hydrodynamics of pulsating active liquids* (2025), arXiv:2407.19955 [cond-mat.soft].
- [10] T. Banerjee, T. Desaleux, J. Ranft, and 'Etienne Fodor, *Contraction waves in pulsating active liquids: From pacemaker to aster dynamics* (2025), arXiv:2509.19024 [cond-mat.stat-mech].
- [11] N. Göth and J. Dzubiella, Collective chemo-mechanical oscillations and cluster waves in communicating colloids, *Commun. Phys.* **8**, 65 (2025).
- [12] W.-j. Zhu, X.-k. Jiang, J.-j. Li, and B.-q. Ai, Directed transport and collective dynamics of pulsing particles in topological lattices, *Phys. Rev. E* **111**, 044123 (2025).
- [13] X.-l. Li and W.-j. Zhu, Spontaneous demixing of a binary cell mixture induced by self-pulsation disparity in confluent tissues, *Phys. Rev. E* **112**, 064407 (2025).
- [14] M. L. Manning, Essay: Collections of deformable particles present exciting challenges for soft matter and biological physics, *Phys. Rev. Lett.* **130**, 130002 (2023).
- [15] K. K. Chiou, J. W. Rocks, C. Y. Chen, S. Cho, K. E. Merkus, A. Rajaratnam, P. Robison, M. Tewari, K. Vogel, S. F. Majkut, B. L. Prosser, D. E. Discher, and A. J. Liu, Mechanical signaling coordinates the embryonic heartbeat, *Proc. Natl. Acad. Sci. USA* **113**, 8939 (2016).
- [16] S. Ishihara, P. Marcq, and K. Sugimura, From cells to tissue: A continuum model of epithelial mechanics, *Phys. Rev. E* **96**, 022418 (2017).
- [17] N. Oyama, T. Kawasaki, H. Mizuno, and A. Ikeda, Glassy dynamics of a model of bacterial cytoplasm with metabolic activities, *Phys. Rev. Res.* **1**, 032038(R) (2019).
- [18] M. F. Staddon, E. M. Munro, and S. Banerjee, Pulsatile contractions and pattern formation in excitable actomyosin cortex, *PLoS Comput. Biol.* **18**, 1 (2022).
- [19] D. Boocock, T. Hirashima, and E. Hannezo, Interplay between mechanochemical patterning and glassy dynamics in cellular monolayers, *PRX Life* **1**, 013001 (2023).
- [20] F. Pérez-Verdugo, S. Banks, and S. Banerjee, Excitable dynamics driven by mechanical feedback in biological tissues, *Commun. Phys.* **7**, 167 (2024).
- [21] W. Tang, M. R. Nejad, A. F. Pegoraro, L. Mahadevan, and M. Guo, *Collective synchrony in confluent, pulsatile epithelia* (2025), arXiv:2507.16772 [cond-mat.soft].
- [22] L. Koehler, E. Sandaltzopoulou, F. Jülicher, and J. Brugués, *Flow-wave coupling synchronizes oscillations in growing active matter* (2026), arXiv:2601.05907 [physics.bio-ph].
- [23] A. Karma, Physics of cardiac arrhythmogenesis, *Annu. Rev. Condens. Matter Phys.* **4**, 313 (2013).
- [24] A. Molavi Tabrizi, A. Mesgarnejad, M. Bazzi, S. Luther, J. Christoph, and A. Karma, Spatiotemporal organization of electromechanical phase singularities during high-frequency cardiac arrhythmias, *Phys. Rev. X* **12**, 021052 (2022).
- [25] W.-J. Rappel, The physics of heart rhythm disorders, *Phys. Rep.* **978**, 1 (2022), the physics of heart rhythm disorders.
- [26] T. Y. Kim, S.-J. Woo, S. min Hwang, J. H. Hong, and K. J. Lee, Cardiac beat-to-beat alternations driven by unusual spiral waves, *Proc. Natl. Acad. Sci. USA* **104**, 11639 (2007).
- [27] A. Bray, Theory of phase-ordering kinetics, *Adv. Phys.* **43**, 357 (1994).
- [28] S. Shankar, A. Souslov, M. J. Bowick, M. C. Marchetti,

- and V. Vitelli, Topological active matter, *Nat. Rev. Phys.* **4**, 380 (2022).
- [29] L. Tubiana, G. P. Alexander, A. Barbensi, D. Buck, J. H. Cartwright, M. Chwastyk, M. Cieplak, I. Coluzza, S. Čopar, D. J. Craik, M. Di Stefano, R. Everaers, P. F. Faísca, F. Ferrari, A. Giacometti, D. Goundaroulis, E. Haglund, Y.-M. Hou, N. Ilieva, S. E. Jackson, A. Japaridze, N. Kaplan, A. R. Klotz, H. Li, C. N. Likos, E. Locatelli, T. López-León, T. Machon, C. Micheletti, D. Michieletto, A. Niemi, W. Niemyska, S. Niewiecz-erzal, F. Nitti, E. Orlandini, S. Pasquali, A. P. Perlin-ska, R. Podgornik, R. Potestio, N. M. Pugno, M. Ravnik, R. Ricca, C. M. Rohwer, A. Rosa, J. Smrek, A. Souslov, A. Stasiak, D. Steer, J. Sułkowska, P. Sułkowski, D. W. L. Sumners, C. Svaneborg, P. Szymczak, T. Tarenzi, R. Travasso, P. Virnau, D. Vlassopoulos, P. Ziherl, and S. Žumer, Topology in soft and biological matter, *Phys. Rep.* **1075**, 1 (2024).
- [30] J. Agudo-Canalejo and E. Tang, Topological phases in discrete stochastic systems, *Rep. Prog. Phys.* **88**, 102601 (2025).
- [31] D. Barkley, Spiral meandering, in *Chemical Waves and Patterns* (Springer Netherlands, 1995) pp. 163–189.
- [32] J. García-Ojalvo and L. Schimansky-Geier, Noise-induced spiral dynamics in excitable media, *Europhys. Lett.* **47**, 298 (1999).
- [33] I. V. Biktasheva and V. N. Biktashev, Wave-particle dualism of spiral waves dynamics, *Phys. Rev. E* **67**, 026221 (2003).
- [34] T. Cameron and J. Davidsen, Induced spiral motion in cardiac tissue due to alternans, *Phys. Rev. E* **86**, 061908 (2012).
- [35] S. F. Pravdin, M. A. Patrakeevev, and A. V. Panfilov, Meander pattern of spiral wave and the spatial distribution of its cycle length, *Phys. Rev. E* **107**, 014215 (2023).
- [36] B. J. Roth, Meandering of spiral waves in anisotropic cardiac tissue, *Physica D: Nonlinear Phenomena* **150**, 127 (2001).
- [37] S. Grill, V. S. Zykov, and S. C. Müller, Feedback-controlled dynamics of meandering spiral waves, *Phys. Rev. Lett.* **75**, 3368 (1995).
- [38] A. S. Mikhailov and K. Showalter, Control of waves, patterns and turbulence in chemical systems, *Phys. Rep.* **425**, 79 (2006).
- [39] L. Giomi, M. J. Bowick, X. Ma, and M. C. Marchetti, Defect annihilation and proliferation in active nematics, *Phys. Rev. Lett.* **110**, 228101 (2013).
- [40] F. C. Keber, E. Loiseau, T. Sanchez, S. J. DeCamp, L. Giomi, M. J. Bowick, M. C. Marchetti, Z. Dogic, and A. R. Bausch, Topology and dynamics of active nematic vesicles, *Science* **345**, 1135 (2014).
- [41] L. Giomi, Geometry and topology of turbulence in active nematics, *Phys. Rev. X* **5**, 031003 (2015).
- [42] S. Shankar, S. Ramaswamy, M. C. Marchetti, and M. J. Bowick, Defect unbinding in active nematics, *Phys. Rev. Lett.* **121**, 108002 (2018).
- [43] L. Angheluta, Z. Chen, M. C. Marchetti, and M. J. Bowick, The role of fluid flow in the dynamics of active nematic defects, *New J. Phys.* **23**, 033009 (2021).
- [44] F. Vafa, Defect dynamics in active polar fluids vs. active nematics, *Soft Matter* **18**, 8087 (2022).
- [45] G. M. La Montagna, S. Bureković, A. Maitra, and C. Nardini, Shape dictates the motion of topological defects in active nematics, *Phys. Rev. E* **113**, L053401 (2026).
- [46] B. N. Radhakrishnan, F. Serafin, T. L. Schmidt, and E. Fodor, Irreversibility in scalar active turbulence: the role of topological defects, *New J. Phys.* **28**, 034601 (2026).
- [47] L. Angheluta, A. Lång, E. Lång, and S. O. Bøe, Full-integer topological defects in polar active matter: From collective migration to tissue patterning, *Annu. Rev. Condens. Matter Phys.* **17**, 305 (2026).
- [48] S.-Z. Lin, F. Jülicher, J. Prost, and J.-F. Rupprecht, Spontaneous flows in active smectics with dislocations, *Eur. Phys. J. Spec. Top.* **235**, 157 (2026).
- [49] E. S. Bililign, F. Balboa Usabiaga, Y. A. Ganan, A. Poncet, V. Soni, S. Magkiriadou, M. J. Shelley, D. Bartolo, and W. T. M. Irvine, Motile dislocations knead odd crystals into whorls, *Nat. Phys.* **18**, 212 (2022).
- [50] Y. Rouzairie and D. Levis, Defect superdiffusion and unbinding in a 2d xy model of self-driven rotors, *Phys. Rev. Lett.* **127**, 088004 (2021).
- [51] Y. Rouzairie, D. J. G. Pearce, I. Pagonabarraga, and D. Levis, Nonreciprocal interactions reshape topological defect annihilation, *Phys. Rev. Lett.* **134**, 167101 (2025).
- [52] See Supplemental Material at [URL will be inserted by publisher] for details on analytical derivations and numerical simulations, which includes Ref. [98].
- [53] P. Curie, Sur la symétrie dans les phénomènes physiques, symétrie d'un champ électrique et d'un champ magnétique, *J. Phys. Theor. Appl.* **3**, 393 (1894).
- [54] P. Reimann, Brownian motors: noisy transport far from equilibrium, *Phys. Rep.* **361**, 57 (2002).
- [55] C. O. Reichhardt and C. Reichhardt, Ratchet effects in active matter systems, *Annu. Rev. Condens. Matter Phys.* **8**, 51 (2017).
- [56] S. Borsley, D. A. Leigh, and B. M. W. Roberts, Molecular ratchets and kinetic asymmetry: Giving chemistry direction, *Angew. Chem. Int. Ed.* **63**, e202400495 (2024).
- [57] I. S. Aranson and L. Kramer, The world of the complex ginzburg-landau equation, *Rev. Mod. Phys.* **74**, 99 (2002).
- [58] J. A. Acebrón, L. L. Bonilla, C. J. Pérez Vicente, F. Ritort, and R. Spigler, The kuramoto model: A simple paradigm for synchronization phenomena, *Rev. Mod. Phys.* **77**, 137 (2005).
- [59] Y. Rouzairie, P. Rahmani, I. Pagonabarraga, F. Peruani, and D. Levis, Activity leads to topological phase transition in 2d populations of heterogeneous oscillators, *Phys. Rev. Lett.* **134**, 188301 (2025).
- [60] D. S. Dean, Langevin equation for the density of a system of interacting langevin processes, *J. Phys. A : Math. Gen.* **29**, L613–L617 (1996).
- [61] E. Fodor and M. C. Marchetti, The statistical physics of active matter: From self-catalytic colloids to living cells, *Physica A* **504**, 106 (2018).
- [62] M. E. Cates and J. Tailleur, Motility-induced phase separation, *Annu. Rev. Condens. Matter Phys.* **6**, 219 (2015).
- [63] H. Chaté, Dry aligning dilute active matter, *Annu. Rev. Condens. Matter Phys.* **11**, 189 (2020).
- [64] A. J. Archer, Dynamical density functional theory for molecular and colloidal fluids: A microscopic approach to fluid mechanics, *J Chem. Phys.* **130**, 014509 (2009).
- [65] A. Manacorda and A. Puglisi, Lattice model to derive the fluctuating hydrodynamics of active particles with inertia, *Phys. Rev. Lett.* **119**, 208003 (2017).
- [66] A. Manacorda and E. Fodor, Diffusive oscillators capture

- the pulsating states of deformable particles, *Phys. Rev. E* **111**, L053401 (2025).
- [67] Y. Zhang, A. Manacorda, and E. Fodor, Species inter-conversion of deformable particles yields transient phase separation, *New J. Phys* **27**, 043023 (2025).
- [68] J. Antonsen, T. M., R. T. Faghih, M. Girvan, E. Ott, and J. Plutig, External periodic driving of large systems of globally coupled phase oscillators, *Chaos* **18**, 037112 (2008).
- [69] L. M. Childs and S. H. Strogatz, Stability diagram for the forced kuramoto model, *Chaos* **18**, 043128 (2008).
- [70] R. Cestnik and A. Pikovsky, Hierarchy of exact low-dimensional reductions for populations of coupled oscillators, *Phys. Rev. Lett.* **128**, 054101 (2022).
- [71] V. Buendía, Mesoscopic theory for coupled stochastic oscillators, *Phys. Rev. Lett.* **134**, 197201 (2025).
- [72] R. Majumder, J. Barré, and S. Gupta, Finite-size fluctuations for stochastic coupled oscillators: A general theory (2025), [arXiv:2510.02448 \[cond-mat.stat-mech\]](https://arxiv.org/abs/2510.02448).
- [73] M. Chatzittofi, R. Golestanian, and J. Agudo-Canalejo, Collective synchronization of dissipatively-coupled noise-activated processes, *New J. Phys.* **25**, 093014 (2023).
- [74] D. Martin, D. Seara, Y. Avni, M. Fruchart, and V. Vitelli, Transition to collective motion in nonreciprocal active matter: Coarse graining agent-based models into fluctuating hydrodynamics, *Phys. Rev. X* **15**, 041015 (2025).
- [75] K. Blom, U. Thiele, and A. c. v. Godec, Local order controls the onset of oscillations in the nonreciprocal ising model, *Phys. Rev. E* **111**, 024207 (2025).
- [76] E. Fodor, C. Nardini, M. E. Cates, J. Tailleur, P. Visco, and F. van Wijland, How far from equilibrium is active matter?, *Phys. Rev. Lett.* **117**, 038103 (2016).
- [77] C. Nardini, E. Fodor, E. Tjhung, F. van Wijland, J. Tailleur, and M. E. Cates, Entropy production in field theories without time-reversal symmetry: Quantifying the non-equilibrium character of active matter, *Phys. Rev. X* **7**, 021007 (2017).
- [78] E. Fodor, R. L. Jack, and M. E. Cates, Irreversibility and biased ensembles in active matter: Insights from stochastic thermodynamics, *Annu. Rev. Condens. Matter Phys.* **13**, 215 (2022).
- [79] B. Liebchen and D. Levis, Collective behavior of chiral active matter: Pattern formation and enhanced flocking, *Phys. Rev. Lett.* **119**, 058002 (2017).
- [80] I. S. Aranson, H. Chaté, and L.-H. Tang, Spiral motion in a noisy complex ginzburg-landau equation, *Phys. Rev. Lett.* **80**, 2646 (1998).
- [81] C. Brito, I. S. Aranson, and H. Chaté, Vortex glass and vortex liquid in oscillatory media, *Phys. Rev. Lett.* **90**, 068301 (2003).
- [82] M. Fruchart and V. Vitelli, Nonreciprocal many-body physics (2026), [arXiv:2602.11111 \[cond-mat.stat-mech\]](https://arxiv.org/abs/2602.11111).
- [83] S. Shankar, V. Raju, and L. Mahadevan, Optimal transport and control of active drops, *Proc. Natl. Acad. Sci. USA* **119**, e2121985119 (2022).
- [84] L. K. Davis, K. Proesmans, and E. Fodor, Active matter under control: Insights from response theory, *Phys. Rev. X* **14**, 011012 (2024).
- [85] R. Garcia-Millan, J. Schüttler, M. E. Cates, and S. A. M. Loos, Optimal closed-loop control of active particles and a minimal information engine, *Phys. Rev. Lett.* **135**, 088301 (2025).
- [86] A. Soriani, E. Tjhung, 'Etienne Fodor, and T. Markovich, Control of active field theories at minimal dissipation (2025), [arXiv:2504.19285 \[cond-mat.stat-mech\]](https://arxiv.org/abs/2504.19285).
- [87] J. Alvarado, E. G. Teich, D. A. Sivak, and J. Bechhoefer, Optimal control in soft and active matter, *Annu. Rev. Condens. Matter Phys.* **17**, 327 (2026).
- [88] V. Krishnan, S. Sinha, and L. Mahadevan, Hamiltonian bridge for scale-dependent optimal control of particles and fields, *Newton* **2**, 100365 (2026).
- [89] M. M. Norton, P. Grover, M. F. Hagan, and S. Fraden, Optimal control of active nematics, *Phys. Rev. Lett.* **125**, 178005 (2020).
- [90] S. Shankar, L. V. D. Scharrer, M. J. Bowick, and M. C. Marchetti, Design rules for controlling active topological defects, *Proc. Natl. Acad. Sci. USA* **121**, e2400933121 (2024).
- [91] S. Ghosh, C. Joshi, A. Baskaran, and M. F. Hagan, Spatiotemporal control of structure and dynamics in a polar active fluid, *Soft Matter* **20**, 7059 (2024).
- [92] S. Ghosh, A. Baskaran, and M. F. Hagan, Achieving designed texture and flows in bulk active nematics using optimal control theory, *J. Chem. Phys.* **162**, 134902 (2025).
- [93] B. C. Geerds, A. Singh, M. Dedenon, D. J. G. Pearce, F. Jülicher, I. F. Sbalzarini, and K. Kruse, Spatiotemporal control of charge +1 topological defects in polar active matter (2025), [arXiv:2511.21359 \[cond-mat.soft\]](https://arxiv.org/abs/2511.21359).
- [94] V. Skogvoll, J. Rønning, M. Salvalaglio, and L. Angheletta, A unified field theory of topological defects and non-linear local excitations, *npj Comput. Mater.* **9**, 122 (2023).
- [95] J. Romano, B. Mahault, and R. Golestanian, Dynamical theory of topological defects i: the multivalued solution of the diffusion equation, *J. Stat. Mech.: Theory Exp.* **2023**, 083211.
- [96] J. Romano, B. Mahault, and R. Golestanian, Dynamical theory of topological defects ii: universal aspects of defect motion, *J. Stat. Mech.: Theory Exp.* **2024**, 033208.
- [97] N. Rana and R. Golestanian, Defect solutions of the non-reciprocal cahn-hilliard model: Spirals and targets, *Phys. Rev. Lett.* **133**, 078301 (2024).
- [98] L.-b. Cai, H. Chaté, Y.-q. Ma, and X.-q. Shi, Dynamical subclasses of dry active nematics, *Phys. Rev. E* **99**, 010601 (2019).